Two-Wheeled Welding Mobile Robot for Tracking a Smooth Curved Welding Path Using Adaptive Sliding-Mode Control Technique

Ngo Manh Dung, Vo Hoang Duy, Nguyen Thanh Phuong, Sang Bong Kim*, and Myung Suck Oh

Abstract: In this paper, a nonlinear controller based on adaptive sliding-mode method which has a sliding surface vector including new boundizing function is proposed and applied to a two-wheeled welding mobile robot (WMR). This controller makes the welding point of WMR achieve tracking a reference point which is moving on a smooth curved welding path with a desired constant velocity. The mobile robot is considered in view of a kinematic model and a dynamic model in Cartesian coordinates. The proposed controller can overcome uncertainties and external disturbances by adaptive sliding-mode technique. To design the controller, the tracking error vector is defined, and then the sliding surface vector including new boundizing function and the adaptation laws are chosen to guarantee that the error vector converges to zero asymptotically. The stability of the dynamic system is shown through the Lyapunov method. In addition, a simple way of measuring the errors by potentiometers is introduced. The simulations and experimental results are shown to prove the effectiveness of the proposed controller.

Keywords: Adaptive control, Lyapunov function, nonlinear control, sliding-mode control, welding mobile robot.

1. INTRODUCTION

Welding automation has been widely used in several manufacturing fields, and one of the most complex applications to manufacturing fields is a welding system based on autonomous robots. Some special welding robots can provide several benefits in certain welding applications. Among them, a welding mobile robot used in line welding application can generates the perfect movements at a certain travel speed, which can produce a consistent weld penetration and weld strength.

In practice, some various robotic welding systems have been developed recently. Kim, *et al.* [1] developed a three dimensional laser vision system for an intelligent shipyard welding robot to detect the welding position and to recognize the 3D shape of the welding environments. Jeon, *et al.* [2] presented the seam tracking and motion control of a two-wheeled welding mobile robot for lattice welding; the control is separated into three driving motions: straight locomotion, turning locomotion, and torch slider control. Kam, *et al.* [3] proposed a mobile welding robot for straight welding path using body positioning sensors and seam tracking sensor. Both of controllers proposed by Jeon and Kam have been successfully applied to the practiced field. Chung, *et al.* [4] proposed a sliding mode control for a mobile robot tracking a smooth-curved path even in the system with known bounded disturbance. In practice, it is very difficult to know the bounded disturbance of the WMR because the pressure of welding arc makes nonlinear disturbance to the WMR. A long welding power cable and CO_2 gas tube are connected from welding system to the WMR of GMAW (gas metal arc weld) process. Furthermore, most of previous sliding mode control methods are applied to mobile robot for tracking a reference path but cannot eliminate the error perpendicular to its heading direction although the angular error of the mobile robot achieves to zero firstly. Therefore, in their simulation and experiment results, the posture of the mobile robot is chosen so that the error perpendicular to its heading direction converges to zero before the angular error converges to zero.

To solve these problems, a nonlinear controller using adaptive sliding-mode method which has a sliding surface vector including new boundizing function is proposed and applied to the WMR for tracking a smooth curved welding path. The new boundizing function is applied to design sliding

Manuscript received May 3, 2006; revised February 1, 2007; accepted February 21, 2007. Recommended by Editorial Board member Sangdeok Park under the direction of Editor Jae-Bok Song. This work was supported by Pukyong National University Research Foundation Grant in 2003.

Ngo Manh Dung, Vo Hoang Duy, Nguyen Thanh Phuong, Sang Bong Kim, and Myung Suck Oh are with the College of Engineering, Pukyong National University, San 100, Yongdang-dong, Nam-gu, Busan 608-739, Korea (e-mails: {vndungtuyen, vhduy, phuongkorea2005}@yahoo.com, {kimsb, msoh}@pknu.ac.kr).

* Corresponding author.

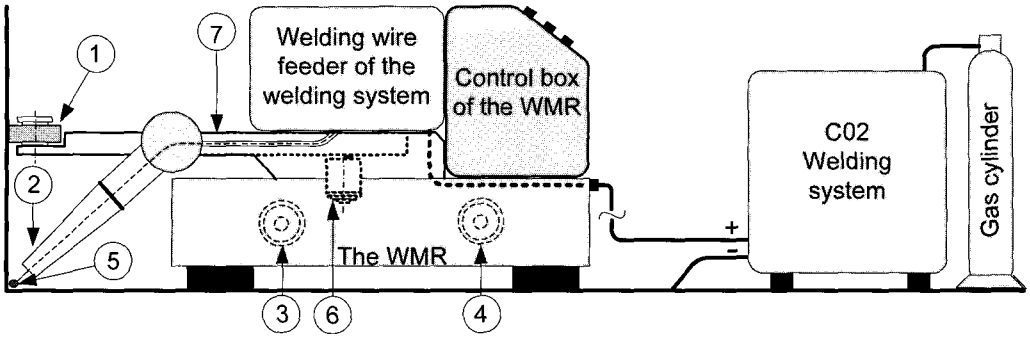

① touch-sensor; ② welding torch; ③,④ left and right wheel driving motors;
⑤ welding point of WMR; ⑥ torch-slide-driving motor; ⑦ torch-slider

Fig. 1. Configuration of the WMR.

surface vector for sliding mode method. The sliding mode method with this sliding surface vector enforces all errors to converge to zero even though the angular error converges to zero firstly. Uncertainties and external disturbances of a system are estimated by adaptive technique. The stability of the dynamic system is shown through the Lyapunov method. In addition, a simple way of measuring the errors by potentiometers is introduced. The simulations and experimental results are shown to prove the effectiveness of the proposed controller.

2. WMR SYSTEM

In this section, the kinematic and dynamic models of the WMR are considered with nonholonomic constraints system. The WMR is modeled under the following assumptions:

(1) The radius of welding curve is sufficiently larger than the turning radius of the WMR,
(2) The robot has two driving wheels for body motion, and those are positioned on an axis passed through the robot's geometric center,
(3) Two passive wheels are installed in front and rear of the bottom of mobile platform for its balance, and their motion can be ignored in the dynamics,
(4) The mass center and the rotation center of the WMR are assumed to be same,
(5) A torch slider is controlled by torch-slide-driving motor and located so as to coincide with the axis through the center of two driving wheels,
(6) A magnet is set up at the bottom of the robot's center to avoid slipping,
(7) The uncertainties and external disturbance are assumed to be unknown and bounded, and also their derivatives are assumed to be zero.

The model of the WMR as shown in Fig. 2 has nomenclatures as the following:

(x, y) :Coordinates of the WMR's center [m]
ϕ :Heading angle of the WMR [rad]
v :Linear velocity of the WMR's center [m/s]

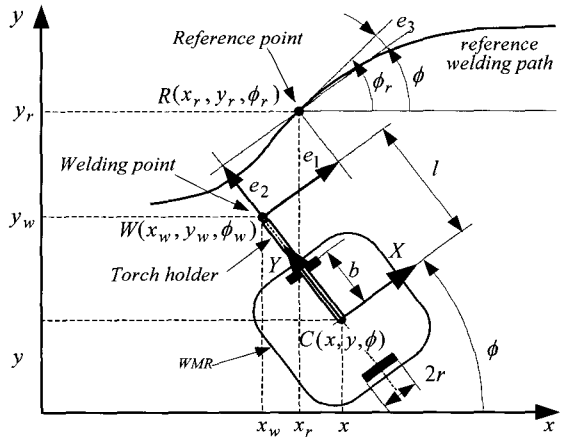

Fig. 2. WMR configuration.

ω :Angular velocity of the WMR's center [rad/s]
ω_{rw}, ω_{lw} :Angular velocities of the right and the left wheels [rad/s]
(x_w, y_w) :Coordinates of the welding point [m]
ϕ_w :Heading angle of the welding point [rad]
v_w :Linear velocity of the welding point [m/s]
ω_w :Angular velocity of the welding point [rad/s]
x_r, y_r :Coordinates of the reference point [m]
v_r :Desired constant welding velocity [m/s]
ω_r :Angular velocity of the reference point [rad/s]
ϕ_r :Reference heading angle [rad]
b :Distance between driving wheel and the symmetric axis [m]
r :Radius of driving wheel [m]
l :Torch holder length [m]
τ :Control input vector [Kgm]
τ_{rw}, τ_{lw} :Torques of the motors acting on the right and the left wheels [Kgm]

m_c :Mass of the body without the driving wheels [Kg]
m_w :Mass of each driving wheel with its motor [Kg]
I_w :Moment of inertia of wheel and its motor about the wheel axis [Kgm^2]
I_m :Moment of inertia of wheel and its motor about the wheel diameter axis [Kgm^2]
I_c :Moment of inertia of the body about the vertical axis through the mass center of the WMR [Kgm^2]
$\mathbf{M(q)}$:Symmetric, positive definite inertia matrix
$\mathbf{V(q,\dot{q})}$:Centripetal and coriolis matrix
$\mathbf{B(q)}$:Input transformation matrix
$\mathbf{A(q)}$:Matrix related with the nonholonomic constraints
$\boldsymbol{\lambda}$:Constraint force vector
$\mathbf{e}$:Tracking error vector
$\mathbf{u}$:Controller vector.

2.1. Kinematic model of the WMR

Consider a robot system having an n-dimensional configuration space with generalized coordinate vector $\mathbf{q}=[q_1,\ldots,q_n]^T$ and subject to m constraints of the following form:

$$\mathbf{A(q)\dot{q}}=0, \tag{1}$$

where $\mathbf{A(q)}\in\mathbf{R}^{m\times n}$ is the matrix associated with the constraints.

As a result, the kinematic model under the nonholonomic constraints in (1) can be derived as follows:

$$\dot{\mathbf{q}}=\mathbf{J(q)z}, \tag{2}$$

where $\mathbf{J(q)}$ is a $n\times(n-m)$ full rank matrix satisfying $\mathbf{J}^T\mathbf{(q)A}^T\mathbf{(q)}=0$, and $\mathbf{z}\in R^{n-m}$ is velocity vector.

Firstly, the posture of mobile robot for the center point of WMR, $C(x, y)$ n the Cartesian space in Fig. 2, is defined as

$$\mathbf{q}=[x,y,\phi]^T. \tag{3}$$

If the mobile robot has nonholonomic constraint that the driving wheels purely roll and do not slip, $\mathbf{A(q)}$ in (1) can be expressed into

$$\mathbf{A(q)}=\begin{bmatrix}-\sin\phi & \cos\phi & 0\end{bmatrix}. \tag{4}$$

From (3)-(4), $n=3$ and $m=1$.

The velocity vector in (2) is defined as

$$\mathbf{z}=\begin{bmatrix}v & \omega\end{bmatrix}^T. \tag{5}$$

In the kinematic model of (2), $\mathbf{J(q)}$ is written as

$$\mathbf{J(q)}=\begin{bmatrix}\cos\phi & 0\\ \sin\phi & 0\\ 0 & 1\end{bmatrix}. \tag{6}$$

The relationship between v, ω nd the angular velocities of two driving wheels is given by

$$\begin{bmatrix}\omega_{rw}\\ \omega_{lw}\end{bmatrix}=\begin{bmatrix}1/r & b/r\\ 1/r & -b/r\end{bmatrix}\begin{bmatrix}v\\ \omega\end{bmatrix}. \tag{7}$$

Secondly, the kinematic equation of the welding point $W(x_w,y_w)$ fixed on the torch holder can be derived from the WMR's center $C(x,y)$ in Fig. 2 as following [6]:

$$\begin{cases}x_w=x-l\sin\phi\\ y_w=y+l\cos\phi\\ \phi_w=\phi.\end{cases} \tag{8}$$

The derivative of (8) yields

$$\begin{bmatrix}\dot{x}_w\\ \dot{y}_w\\ \dot{\phi}_w\end{bmatrix}=\begin{bmatrix}\cos\phi & -l\cos\phi\\ \sin\phi & -l\sin\phi\\ 0 & 1\end{bmatrix}\begin{bmatrix}v\\ \omega\end{bmatrix}+\begin{bmatrix}-\dot{l}\sin\phi\\ \dot{l}\cos\phi\\ 0\end{bmatrix}, \tag{9}$$

where l is controlled by torch-slide-driving motor.

The coordinates (x_r, y_r) and the reference heading angle ϕ_r of the reference point R, which is moving on the reference welding path with the desired constant velocity of v_r, satisfies the following equations:

$$\begin{cases}\dot{x}_r=v_r\cos\phi_r\\ \dot{y}_r=v_r\sin\phi_r\\ \dot{\phi}_r=\omega_r.\end{cases} \tag{10}$$

In Fig. 2, the error vector $\mathbf{e}=[e_1,e_2,e_3]^T$ is defined as the difference between the welding point of WMR and the reference point. The relationship of the error vector between the global coordinate and the WMR's coordinate can be expressed as follows:

$$\begin{bmatrix}e_1\\ e_2\\ e_3\end{bmatrix}=\begin{bmatrix}\cos\phi & \sin\phi & 0\\ -\sin\phi & \cos\phi & 0\\ 0 & 0 & 1\end{bmatrix}\begin{bmatrix}x_r-x\\ y_r-y\\ \phi_r-\phi\end{bmatrix}. \tag{11}$$

The first derivative of error vector yields

$$\begin{bmatrix}\dot{e}_1\\ \dot{e}_2\\ \dot{e}_3\end{bmatrix}=\begin{bmatrix}-1 & e_2+l\\ 0 & -e_1\\ 0 & -1\end{bmatrix}\begin{bmatrix}v\\ \omega\end{bmatrix}+\begin{bmatrix}v_r\cos e_3\\ v_r\sin e_3-\dot{l}\\ \omega_r\end{bmatrix}. \tag{12}$$

2.2. Dynamic model of the WMR

The dynamic equations of the mechanical system under nonholonomic constraints in (1) can be described by Euler-Lagrange formulation as follows [5]:

$$\mathbf{M(q)}\ddot{\mathbf{q}} + \mathbf{V(q,\dot{q})}\dot{\mathbf{q}} = \mathbf{B(q)}\boldsymbol{\tau} - \mathbf{A}^T\mathbf{(q)}\boldsymbol{\lambda}, \tag{13}$$

where $\mathbf{M(q)} \in \mathbf{R}^{n\times n}$ is a symmetric positive definite inertia matrix; $\mathbf{V(q,\dot{q})} \in \mathbf{R}^{n\times n}$, a centripetal and Coriolis matrix; $\mathbf{B(q)} \in \mathbf{R}^{n\times r}$, an input transformation matrix; $\mathbf{A(q)} \in \mathbf{R}^{m\times n}$, a matrix of nonholonomic constraints; $\boldsymbol{\tau} \in \mathbf{R}^r$, a control input vector; and $\boldsymbol{\lambda} \in \mathbf{R}^m$, a constraint force vector. For simplicity of analysis, it is assumed that $r = n - m$.

Differentiating (2), substituting this result in (13) and multiplying by $\mathbf{J}^T$, the constraint matrix $\mathbf{A}^T\mathbf{(q)}\boldsymbol{\lambda}$ is eliminated. Dynamics in platform system of the nonholonomic mobile robot with the constraint in (1) is as follows [5]:

$$\mathbf{J}^T\mathbf{M}\mathbf{J}\dot{\mathbf{z}} + \mathbf{J}^T(\mathbf{M}\dot{\mathbf{J}} + \mathbf{V}\mathbf{J})\mathbf{z} = \mathbf{J}^T\mathbf{B}\boldsymbol{\tau}. \tag{14}$$

Multiplying by $(\mathbf{J}^T\mathbf{B})^{-1}$, (14) can be rewritten as follows:

$$\bar{\mathbf{M}}\mathbf{(q)}\dot{\mathbf{z}} + \bar{\mathbf{V}}\mathbf{(q,\dot{q})}\mathbf{z} = \boldsymbol{\tau}, \tag{15}$$

where

$$\bar{\mathbf{M}}\mathbf{(q)} = (\mathbf{J}^T\mathbf{B})^{-1}\mathbf{J}^T\mathbf{M}\mathbf{J} \in \mathbf{R}^{r\times(n-m)},$$
$$\bar{\mathbf{V}}\mathbf{(q,z)} = (\mathbf{J}^T\mathbf{B})^{-1}\mathbf{J}^T(\mathbf{M}\dot{\mathbf{J}} + \mathbf{V}\mathbf{J}) \in \mathbf{R}^{r\times(n-m)}.$$

In this paper, the behavior of the welding mobile robot in the presence of external disturbances $\boldsymbol{\tau}_d \in \mathbf{R}^{r\times 1}$ is considered. The real dynamic equation of the welding mobile robot with the external disturbances can be derived from (15) as follows:

$$\bar{\mathbf{M}}\mathbf{(q)}\dot{\mathbf{z}} + \bar{\mathbf{V}}\mathbf{(q,\dot{q})}\mathbf{z} + \boldsymbol{\tau}_\mathbf{d} = \boldsymbol{\tau}. \tag{16}$$

It is assumed that the disturbance vector can be expressed as a multiplier of matrix $\bar{\mathbf{M}}\mathbf{(q)}$ as the following:

$$\boldsymbol{\tau}_\mathbf{d} = \bar{\mathbf{M}}\mathbf{(q)}\mathbf{f}, \tag{17}$$

where $\mathbf{f} \in \mathbf{R}^{(n-m)\times 1}$ is the vector of uncertainty and the external disturbance of system.

By a feedback linearization of the system, the controller vector $\mathbf{u} \in \mathbf{R}^{(n-m)\times 1}$ is defined by computed-torque method as follows [5]:

$$\boldsymbol{\tau} = \bar{\mathbf{M}}\mathbf{(q)}\dot{\mathbf{z}}_\mathbf{r} + \bar{\mathbf{V}}\mathbf{(q,\dot{q})}\mathbf{z} + \bar{\mathbf{M}}\mathbf{(q)}\mathbf{u}, \tag{18}$$

where $\mathbf{z}_r \in \mathbf{R}^{(n-m)\times 1}$ is reference input vector.

From (16), (17) and (18), (19) is obtained.

$$\mathbf{f} = \mathbf{u} - (\dot{\mathbf{z}} - \dot{\mathbf{z}}_\mathbf{r}) \tag{19}$$

In this paper, when $\mathbf{q} = [x, y, \phi]^T$ is taken, that is, $n = 3$, $m = 1$ and $r = 2$. The followings are obtained from (16)-(19).

$$\bar{\mathbf{V}} = \begin{bmatrix} 0 & \frac{r^2}{2b}m_c d\dot{\phi} \\ -\frac{r^2}{2b}m_c d\dot{\phi} & 0 \end{bmatrix},$$
$$\bar{\mathbf{M}} = \begin{bmatrix} \frac{r^2}{4b^2}(mb^2 + I) + I_w & \frac{r^2}{4b^2}(mb^2 - I) \\ \frac{r^2}{4b^2}(mb^2 - I) & \frac{r^2}{4b^2}(mb^2 + I) + I_w \end{bmatrix}, \tag{20}$$
$$\boldsymbol{\tau} = [\tau_{rw} \quad \tau_{lw}]^T, \quad m = m_c + 2m_w,$$
$$I = m_c d^2 + 2m_w b^2 + I_c + 2I_m,$$
$$\mathbf{z}_r = [v_r \quad \omega_r]^T, \quad \mathbf{f} = [f_1 \quad f_2]^T.$$

3. ADAPTIVE SLIDING-MODE CONTROLLER DESIGN

Our objective is to design a controller so that the welding point W tracks the reference point R at a desired constant velocity of welding v_r. So the designed controller makes the WMR achieve $\mathbf{e} \to 0$ as $t \to \infty$.

In this paper, the WMR is controlled in two cases: fixed torch slider and controllable torch slider. In the second case, the length of the torch is controlled by torch-slide-driving motor.

3.1. Controller design for fixed torch

In this case, the $\dot{l}$ is equal to zero. To design an adaptive sliding mode controller, the sliding surfaces are defined as follows:

$$\mathbf{s} = \begin{bmatrix} s_1 \\ s_2 \end{bmatrix} = \begin{bmatrix} \dot{e}_1 + k_1 e_1 \\ \dot{e}_3 + k_2 e_3 + k_3 \psi(e_3) e_2 \end{bmatrix}, \tag{21}$$

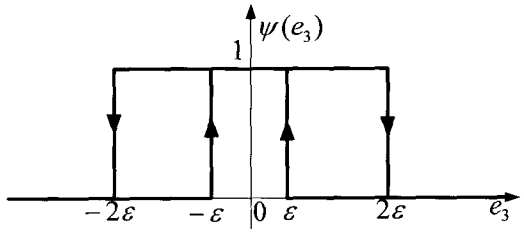

Fig. 3. Characteristic of $\psi(\cdot)$ function.

where k_1, k_2 and k_3 are positive constant values; a boundizing function $\psi(\cdot)$ is defined as follows:

$$\psi(e_3)=\begin{cases}0\rightarrow 1 & \text{if } |e_3|\le\varepsilon\\ 1\rightarrow 0 & \text{if } |e_3|\ge 2\varepsilon\\ \text{no change} & \text{if } \varepsilon<|e_3|<2\varepsilon,\end{cases} \tag{22}$$

where ε is positive constant value. "No change" means the value of $\psi(\cdot)$ function continuously keeps its value at point $e_3=\pm\varepsilon$ or $e_3=\pm 2\varepsilon$ before e_3 enters into $\varepsilon<|e_3|<2\varepsilon$.

On the sliding surface vector $(\mathbf{s}=0)$, the followings are obtained from (21):

$$\dot{e}_1=-k_1e_1, \tag{23}$$

$$\dot{e}_3=-k_2e_3-k_3\,\psi(e_3)\,e_2. \tag{24}$$

In (23), if e_1 is positive, $\dot{e}_1$ is negative, and vice versa. Thus, the equilibrium point of e_1 converges to zero as $t\rightarrow\infty$. It means the error $e_1\rightarrow 0$ as $t\rightarrow\infty$ along the sliding surface $(s_1=0)$.

Because the configuration of the WMR has the welding point which is fixed on the axis through the two contact points between driving wheels and floor, the error e_2 can be eliminated via e_3. But, in the case of $e_3=0$, the value of e_2 is constant because WMR is running parallel with reference trajectory. For that result, the error e_3 and its derivative in (24) cannot be zero in order to eliminate the error e_2 when the error $e_2\neq 0$.

In case of $|e_3|>\varepsilon$, firstly, $\psi(\cdot)$ is inactive until $|e_3|\le\varepsilon$. So (24) becomes $\dot{e}_3=-k_2e_3$. Similarly with (23), e_3 converges into $(-\varepsilon\ \ \varepsilon)$. Secondly, when $|e_3|<\varepsilon$, $\psi(\cdot)$ is active in $|e_3|<2\varepsilon$. So (24) becomes $\dot{e}_3=-k_2e_3-k_3e_2$. This result makes error e_3 be changed according to the value of error e_2. Based on the specific configuration of the WMR, this phenomenon forces $e_2\rightarrow 0$. When $e_2=0$, (24) becomes $\dot{e}_3=-k_2e_3$. So $e_3\rightarrow 0$ as $t\rightarrow\infty$. The convergence to zero of error vector $\mathbf{e}$ is shown clearly in Figs. 10, 11 and 14 of the simulation results section.

The following procedure is to design an adaptation law vector $\dot{\hat{\boldsymbol{\rho}}}$ and a controller vector $\mathbf{u}$ which make the sliding surface be stabilized and converge to zero as $t\rightarrow\infty$.

Firstly, the adaptation law is proposed as the following:

$$\dot{\hat{\boldsymbol{\rho}}}=\boldsymbol{\xi}^{-1}\mathbf{s}(t), \tag{25}$$

where $\hat{\boldsymbol{\rho}}=\begin{bmatrix}\hat{\rho}_1 & \hat{\rho}_2\end{bmatrix}^T$ is an estimate value of $\mathbf{f}=\begin{bmatrix}f & f_2\end{bmatrix}^T$; $\boldsymbol{\xi}^{-1}=\begin{bmatrix}\xi_{11}^{-1} & 0\\ 0 & \xi_{22}^{-1}\end{bmatrix}$ is positive definite matrix which is denoted as an adaptation gain.

The estimation error is defined as follows:

$$\tilde{\boldsymbol{\rho}}=\mathbf{f}-\hat{\boldsymbol{\rho}}\ \Rightarrow\ \hat{\boldsymbol{\rho}}=\mathbf{f}-\tilde{\boldsymbol{\rho}}. \tag{26}$$

Secondly, the controller vector $\mathbf{u}$ is chosen as follows:

$$\begin{aligned}\mathbf{u}&=\begin{bmatrix}u_1 & u_2\end{bmatrix}^T\\ &=\begin{bmatrix}(v_r\sin e_3-e_1\omega+\dot{l})\omega+(e_2+l)\dot{\omega}-v_r\sin e_3(\omega_r-\omega)\\ 0\end{bmatrix}\\ &\quad+\begin{bmatrix}k_1[e_2+l]\omega-v+v_r\cos e_3\\ k_2(\omega_r-\omega)+k_3\psi(e_3)(v_r\sin e_3-\dot{l}-e_1\omega\end{bmatrix}\\ &\quad+\mathbf{Qs}+|\mathbf{P}|\,\mathrm{sgn}(\mathbf{s}).\end{aligned} \tag{27}$$

From (12), the (27) can be rewritten as follows:

$$\begin{aligned}\mathbf{u}&=\begin{bmatrix}(\dot{e}_2+\dot{l})\omega+(e_2+l)\dot{\omega}-v_r\dot{e}_3\sin e_3\\ 0\end{bmatrix}\\ &\quad+\begin{bmatrix}k_1\dot{e}_1\\ k_2\dot{e}_3+k_3\,\psi(e_3)\,\dot{e}_2\end{bmatrix}+\mathbf{Qs}+|\mathbf{P}|\,\mathrm{sgn}(\mathbf{s}),\end{aligned} \tag{28}$$

where $\mathbf{Q}=\begin{bmatrix}q_{11} & 0\\ 0 & q_{22}\end{bmatrix}$ and $|\mathbf{P}|=\begin{bmatrix}|\hat{\rho}_1| & 0\\ 0 & |\hat{\rho}_2|\end{bmatrix}$ are positive definite matrices.

Theorem: The above controller vector $\mathbf{u}$ and adaptation law vector $\dot{\hat{\boldsymbol{\rho}}}$ with the assumption (7) make the sliding surfaces in (21) be stabilized and converge to zero as $t\rightarrow\infty$. From (21)-(24), this implies that the error vector $\mathbf{e}\rightarrow 0$ as $t\rightarrow\infty$.

Proof: Because the welding velocity is constant, $\dot{v}_r=0$. From (12), the first and the second derivatives of e_1 and e_3 yield

$$\begin{bmatrix}\dot{e}_1\\ \dot{e}_3\end{bmatrix}=\begin{bmatrix}v_r\cos e_3+(e_2+l)\omega-v\\ -(\omega-\omega_r)\end{bmatrix}, \tag{29}$$

$$\begin{aligned}\begin{bmatrix}\ddot{e}_1\\ \ddot{e}_3\end{bmatrix}&=\begin{bmatrix}(\dot{e}_2+\dot{l})\omega+(e_2+l)\dot{\omega}-v_r\dot{e}_3\sin e_3\\ 0\end{bmatrix}\\ &\quad-\begin{bmatrix}(\dot{v}-\dot{v}_r)\\ (\dot{\omega}-\dot{\omega}_r)\end{bmatrix}.\end{aligned} \tag{30}$$

Using (19) and (28), (30) can be rewritten as follows:

$$\begin{bmatrix}\ddot{e}_1\\ \ddot{e}_3\end{bmatrix}=\mathbf{f}-\mathbf{u}+\begin{bmatrix}(\dot{e}_2+\dot{l})\omega+(e_2+l)\dot{\omega}-v_r\dot{e}_3\sin e_3\\ 0\end{bmatrix}, \quad (31)$$

$$\begin{bmatrix}\ddot{e}_1\\ \ddot{e}_3\end{bmatrix}=\mathbf{f}-\mathbf{Qs}-|\mathbf{P}|\mathrm{sgn}(\mathbf{s})-\begin{bmatrix}k_1\dot{e}_1\\ k_2\dot{e}_3+k_3\,\psi(e_3)\dot{e}_2\end{bmatrix}. \quad (32)$$

From (21) and (32), the first derivative of the sliding surfaces yields

$$\dot{\mathbf{s}}=\begin{bmatrix}\ddot{e}_1\\ \ddot{e}_3\end{bmatrix}+\begin{bmatrix}k_1\dot{e}_1\\ k_2\dot{e}_3+k_3\,\psi(e_3)\dot{e}_2\end{bmatrix}=\mathbf{f}-\mathbf{Qs}-|\mathbf{P}|\mathrm{sgn}(\mathbf{s}). \quad (33)$$

The following Lyapunov function is chosen as

$$V=\frac{1}{2}\mathbf{s}^T\mathbf{s}+\frac{1}{2}\tilde{\boldsymbol{\rho}}^T\boldsymbol{\xi}\tilde{\boldsymbol{\rho}}\geq 0. \quad (34)$$

Its derivative yields

$$\dot{V}=\mathbf{s}^T\dot{\mathbf{s}}+\tilde{\boldsymbol{\rho}}^T\boldsymbol{\xi}\dot{\tilde{\boldsymbol{\rho}}}. \quad (35)$$

The derivative of (26) and the assumption (7) yields

$$\dot{\hat{\boldsymbol{\rho}}}=\dot{\mathbf{f}}-\dot{\tilde{\boldsymbol{\rho}}}=-\dot{\tilde{\boldsymbol{\rho}}}. \quad (36)$$

Therefore, the derivative of Lyapunov function is as follows:

$$\begin{aligned}\dot{V}&=-\mathbf{s}^T\mathbf{Qs}+\mathbf{s}^T\mathbf{f}-\mathbf{s}^T|\mathbf{P}|\mathrm{sgn}(\mathbf{s})+(\mathbf{f}^T-\hat{\boldsymbol{\rho}}^T)\boldsymbol{\xi}\dot{\tilde{\boldsymbol{\rho}}}\\&=-\mathbf{s}^T\mathbf{Qs}-(|\mathbf{s}^T\hat{\boldsymbol{\rho}}|-\mathbf{s}^T\hat{\boldsymbol{\rho}})\leq-\mathbf{s}^T\mathbf{Qs}\leq 0.\end{aligned} \quad (37)$$

Since $V\geq 0$ and $\dot{V}$ is negative semi-definite, by Barbalat's lemma, $\mathbf{s}\to 0$ as $t\to\infty$. From (25), this implies that $\hat{\boldsymbol{\rho}}$ has constant value as $t\to\infty$. From (21), (23), and (24), this implies that $\mathbf{e}\to 0$ as $t\to\infty$. When $\mathbf{e}\to 0$, the welding point of the WMR achieves tracking a reference point which is moving on a smooth welding path at a specified constant velocity. □

3.2. Controller design for controllable torch

In the welding application field, the welding velocity is very slow, which is 7.5mm/s. Therefore, if there exists an error e_2, the WMR takes a long time to converge the errors vector $\mathbf{e}$ to zero. To solve this problem, a sliding controllable torch holder is replaced for fixed torch holder in the previous case. A torch-slide-driving motor is used to drive the sliding torch. In this case, the length l is changeable so ($\dot{l}\neq 0$). Furthermore, a new update law $\dot{l}$ for sliding controllable torch is designed.

The same concept with the previous case, a new sliding surface vector $\mathbf{s}$ and a new controller vector $\mathbf{u}$ are obtained from (21)-(28) with ($\dot{l}\neq 0$).

To design an update law for sliding controllable torch, a Lyapunov function candidate for error e_2 as follows:

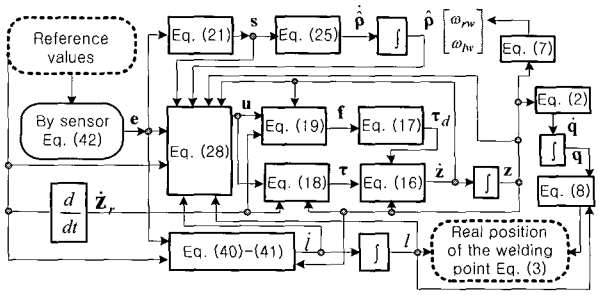

Fig. 4. Block diagram for tracking a reference welding path.

$$V_m=\frac{1}{2}e_2^2\geq 0, \quad (38)$$

$$\dot{V}_m=e_2\dot{e}_2=e_2(-e_1\omega+v_r\sin e_3-\dot{l}). \quad (39)$$

The update law for sliding controllable torch is achieved by $\dot{V}_m\leq 0$ as follows:

$$\dot{l}=v_r\sin e_3+k_4e_2-e_1\omega. \quad (40)$$

To avoid overshot controlling of e_2, the maximum speed of sliding torch has to be limited by saturation function below

$$sat(\dot{l})=\begin{cases}\dot{l} & if \quad |\dot{l}|<\delta(v_r)\\ \delta(v_r) & if \quad |\dot{l}|>\delta(v_r),\end{cases} \quad (41)$$

where $\delta(v_r)$ is positive value which depends on v_r is chosen by designer.

Clearly, $V\geq 0$, $V_m\geq 0$, $\dot{V}\leq 0$ and $\dot{V}_m\leq 0$ with the proposed controller vector $\mathbf{u}$, adaptation law vector $\dot{\hat{\boldsymbol{\rho}}}$ and update law $\dot{l}$ are satisfied. So the error vector $\mathbf{e}\to 0$ as $t\to\infty$.

For tracking a reference welding path, based on the error vector which is derived from touch sensor, the angular velocities of left and right wheels of the WMR are obtained by the following block diagram Fig. 4.

4. SIMULATION AND EXPERIMENTAL RESULTS

To verify the effectiveness of the proposed controllers, the simulation has been done for the two cases of fixed torch and controllable torch with a smooth curved reference welding path. Fig. 5 shows the reference curve welding path with straight line of $L_1=112$mm, arc curve line of $(R_1=95.5\text{mm}, 45°)$, straight line of $L_2=36$mm, arc curve line of

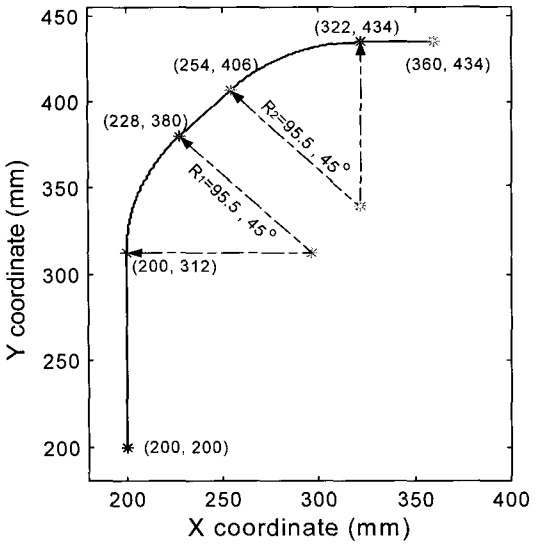

Fig. 5. Smooth curved reference welding path.

$(R_2 = 95.5\text{mm}, 45°)$ and straight line of $L_3 = 38\text{mm}$. The simulation results show the error vector converges to zero faster in the case of controllable torch than in the case of fixed torch. Furthermore, the experiment has been done for the controllable torch case.

4.1. Hardware of the whole system

Fig. 6 shows configuration of the control system. The control system is based on the integration of two microcontroller PIC18F452s: one is used for two servo DC motor control signal of left wheel and right wheel. Another is used for servo torch slider controller and main center processor unit (CPU). The three servo controllers are controlled by CPU. The main controller functionalized as master links to the three servo controllers via I2C communication.

The two A/D ports of the CPU are connected with the two potentiometers for sensing the errors as considered in Section 4.2. Two microcontrollers PIC18F452s are operated with the clock frequency 40MHz. The servo DC motor has 16-bit register for the capture module which is used for receiving signal from motor-encoder and PWM module for controlling the PWM of DC motor. The sampling time of control

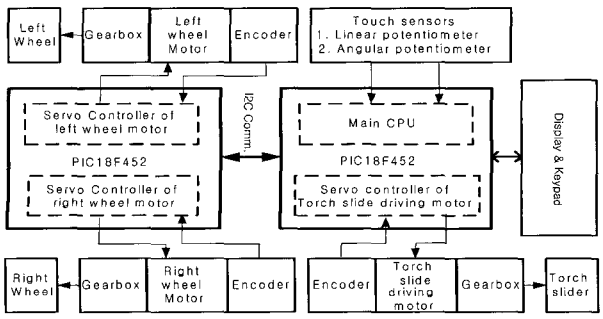

Fig. 6. Configuration of the control system.

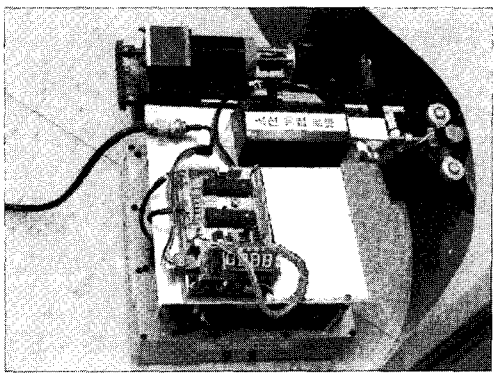

Fig. 7. Experimental welding mobile robot.

system is 10ms.

The experimental WMR is shown in Fig. 7 and its dimensions are shown in Table 1.

4.2. Measurement of the errors e_1, e_2, e_3

In order to measure the components of the error vector **e**, a simple measurement scheme using potentiometers is shown in Fig. 8. Two rollers are placed at points O_2 and O_3. Two sensors for measuring the errors are needed. That is, they are one linear sensor for measuring d_s and one rotating sensor for measuring the angle between the torch and the tangent line of the wall at the welding point.

From Fig. 8, the relation of the components of error vector **e** can be expressed as follows:

$$\begin{aligned} e_1 &= -r_s \sin e_3, \\ e_2 &= d_s + r_s |\cos e_3|, \\ e_3 &= \angle(O_1O_3, O_1E) - \pi/2, \end{aligned} \tag{42}$$

where O_2 and O_3 are the center points of rotor O_2 and O_3 respectively, O_1 is the center point of O_2O_3, E is the point on torch holder, r_s is the radius of the roller, d_s is the length measured by the linear potentiometer, and e_3 is the angle measured by the rotating potentiometer. In Fig. 8, the welding path is a line. When the welding path is a curve, (42)

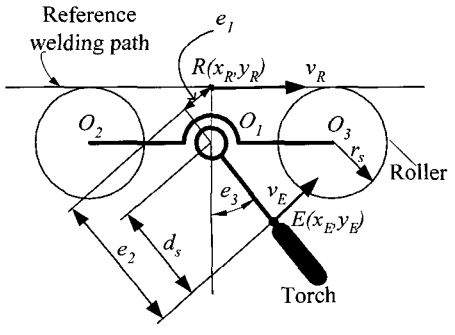

Fig. 8. Scheme for measuring the error vector **e**.

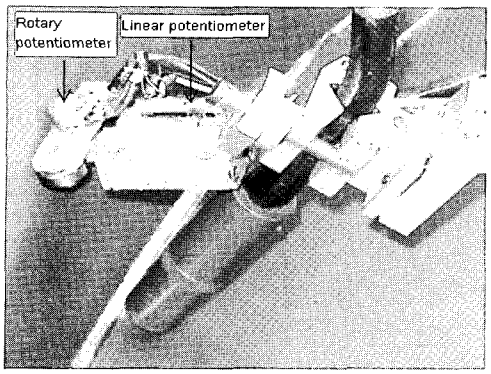

Fig. 9. Touch sensor.

is also valid if the distance O_2O_3 is sufficiently small and the radius of the welding path is enough large.

4.3. Simulation and experimental results

The welding speed in this application is $v_r = 7.5$ mm/s. The sampling time of control system is 10ms. The designed parameters are as follows: $k_1 = 20\text{s}^{-1}$, $k_2 = 6\text{s}^{-1}$, $k_3 = 120\text{s}^{-1}$, $\varepsilon = 3^\circ$, $\mathbf{Q} = [(30\text{s}^{-1}\ 0); (0\ 10\text{s}^{-1})]$, the initial estimated value $\hat{\boldsymbol{\rho}}_0 = [(6\text{mms}^{-2}\ \text{deg s}^{-2})]$, the adaptation gain vector $\xi = [(10\text{s}^{-2}\ 0); (0\ 10\text{s}^{-2})]$, $k_4 = 0.5\text{s}^{-1}$ and $\delta(v_r) = 0.05\text{ms}^{-1}$.

Table 1. Parameter values of the WMR.

Parameter	Value	Unit
b	0.105	m
r	0.025	m
m_w	0.2	Kg
I_w	3.75×10^{-4}	Kgm^2
l	0.145	m
m_c	10	Kg
I_c	0.2081	Kgm^2
I_m	4.96×10^{-4}	Kgm^2

Table 2. Initial values for the simulation and experiment.

Parameter	Value	Unit
x_r	0.2	m
x_w	0.204	m
v	0	m/s
ϕ_r	$\pi/2$	rad
l	0.145	m
y_r	0.200	m
y_w	0.195	m
ω	0	rad/s
ϕ	84° or 96°	deg
ω_r	0	rad/s

Two initial error vectors are considered as follows: $\mathbf{e}_{01} = (5.4\text{mm}, 4.9\text{mm}, -6\text{deg})$ and $\mathbf{e}_{02} = (4.6\text{mm}, 6\text{ mm}, 6\text{deg})$.

The WMR's parameters and the initial values for the simulation are given in Tables 1 and 2.

4.3.1 Simulation results for the case of fixed torch

In this case, the tracking error vector has been simulated with two different initial error vectors $\mathbf{e}_{01}$ and $\mathbf{e}_{02}$ as shown in Figs. 10 and 11.

Fig. 10 shows that firstly, $\psi(\cdot)$ in (24) is un-active and the error e_3 intends to converge to bounded limit $(-\varepsilon\ \ \varepsilon) = (-3^o\ \ 3^o)$. Secondly, when $|e_3| \le \varepsilon$, $\psi(\cdot)$ is active in the bounded $(-2\varepsilon\ \ 2\varepsilon)$ at this time $e_2 \neq 0$. So e_3 is changed in order to converge e_2 to zero. When $e_2 \to 0$, the part $[k_3\psi(e_3)e_2] \to 0$, too. Therefore, error e_3 is decreased as e_2 is decreased. Finally, when $e_2 \to 0$, $e_3 \to 0$.

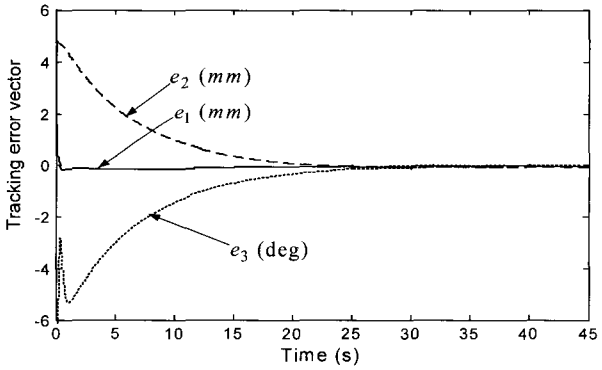

Fig. 10. Tracking error vector with initial error vector $\mathbf{e}_{01}$.

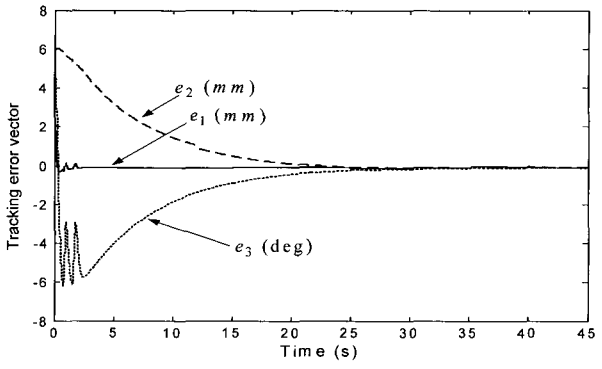

Fig. 11. Tracking error vector with initial error vector $\mathbf{e}_{02}$.

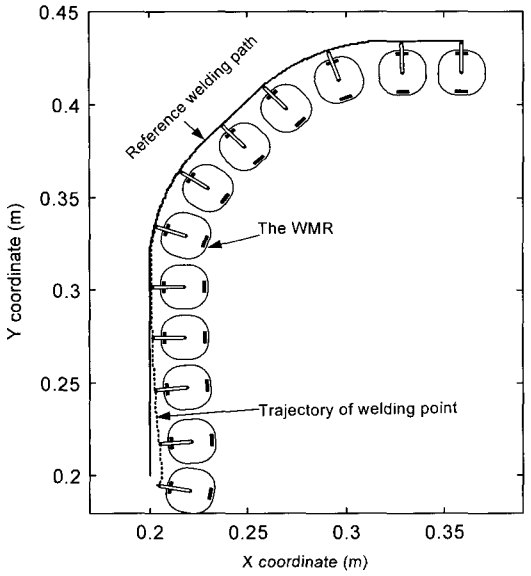

Fig. 12. Movement of the WMR with fixed torch by initial error vector $\mathbf{e}_{02}$.

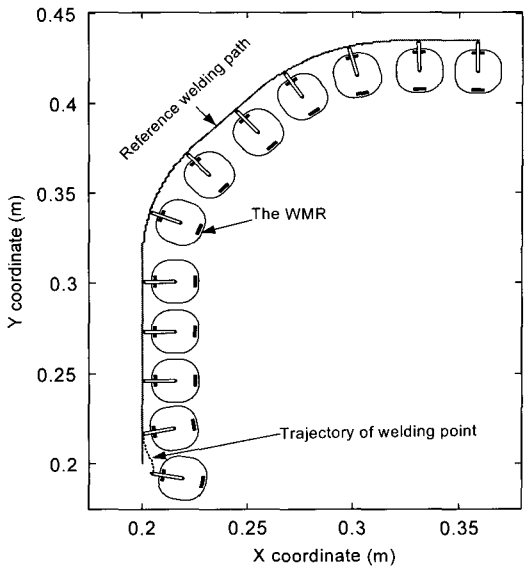

Fig. 13. Movement of the WMR with torch controllable by initial error vector $\mathbf{e}_{02}$.

Fig. 11 shows that firstly, there is $e_2 \neq 0$ when e_3 converges to bounded limit $(-\varepsilon\ \varepsilon)$. Due to the characteristic of $\psi(e_3)$, e_3 is changed in order to converge e_2 to zero. In this case if the error $e_3 > 2\varepsilon$, $\psi(e_3)$ is un-active. So e_3 approaches into bounded limit $(-\varepsilon\ \varepsilon)$ again. This phenomenon forces the error vector $\mathbf{e}$ to be zero as $t \to 0$.

Fig. 12 shows the movement of the WMR along the reference welding path with the initial error vector $\mathbf{e}_{02}$. The proposed controller makes the error vector $\mathbf{e} \to 0$ as $t \to 0$ and the WMR track the whole reference welding path very well and tightly. In Fig. 12, it nearly takes about 25 seconds to converge the vector error $\mathbf{e}$ to zero. So this disadvantage is overcome by controllable torch.

4.3.2 Simulation and experimental results for the case of controllable torch

The WMR with controllable torch moves along the reference welding path with the same initial error vector $\mathbf{e}_{02}$ as shown in Fig. 13.

In the case of controllable torch, the error vector $\mathbf{e}$ converges to zero faster than in the case of fixed torch as shown in Fig. 14. After about 5 seconds, all the errors converge to zero during the welding process.

Fig. 15 shows the simulation and experiment results for tracking error vector with initial error vector $\mathbf{e}_{01}$ during 12 seconds at beginning. It shows that the experiment result of the tracking error vector is bounded along the simulation result.

Fig. 16 shows the angular velocity of the center of the WMR ω for tracking straight line, arc line,

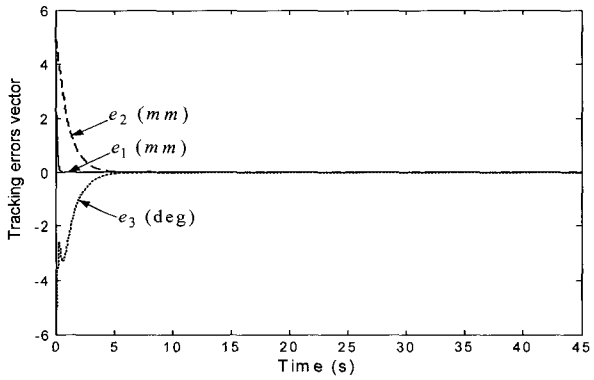

Fig. 14. Tracking error vector with initial error vector $\mathbf{e}_{01}$.

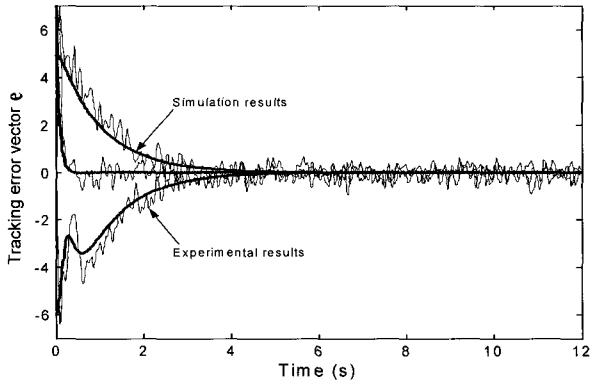

Fig. 15. Simulation and experimental results with initial error vector $\mathbf{e}_{01}$ for 12 seconds at beginning.

straight line, arc line and straight line of the fully reference welding path. The angular velocity ω has a little larger chattering during tracking the arc line

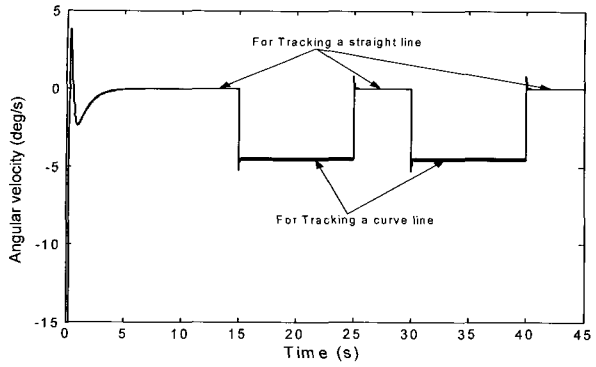

Fig. 16. Angular velocity of center of the WMR.

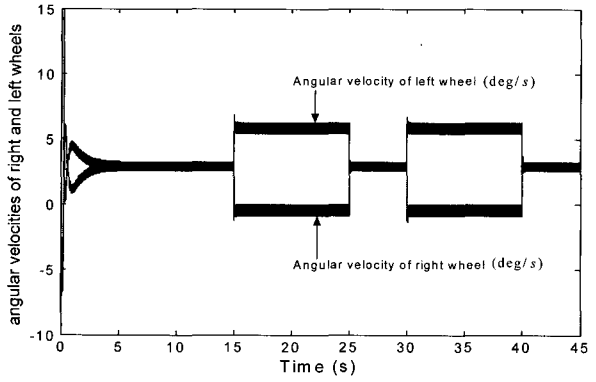

Fig. 17. Angular velocities of right and left wheels of the WMR.

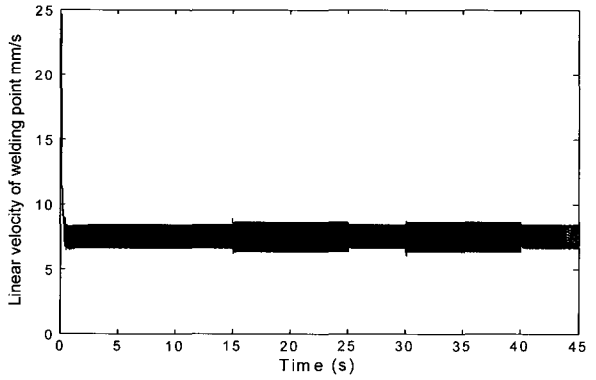

Fig. 18. Linear velocity of welding point.

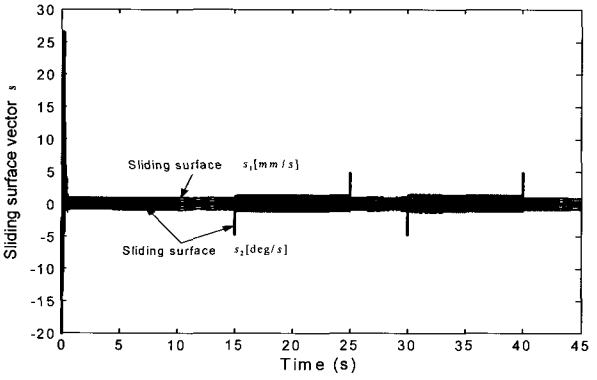

Fig. 19. Sliding surface vector **s**.

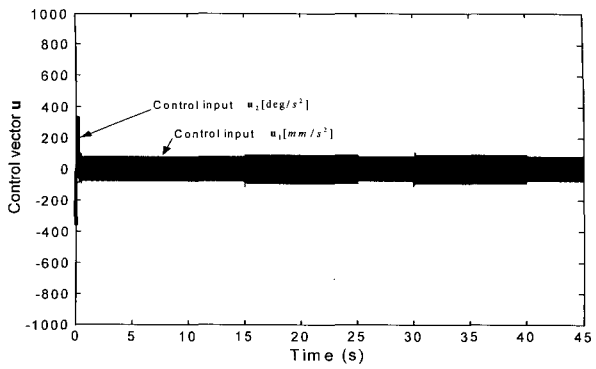

Fig. 20. Controller vector **u**.

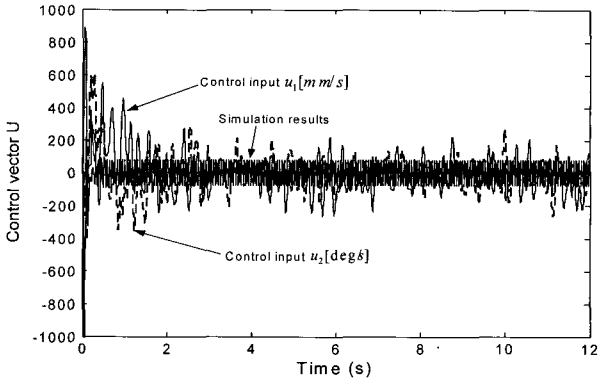

Fig. 21. Experimental results of controller vector **u** for 12 seconds at beginning.

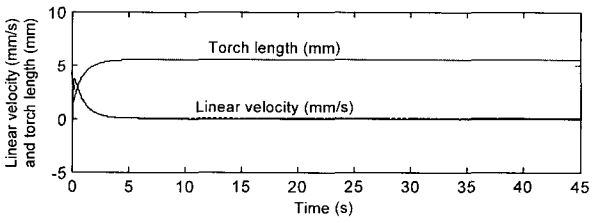

Fig. 22. Linear velocity of torch slider $\dot{l}$ [mm/s] and torch length l [mm].

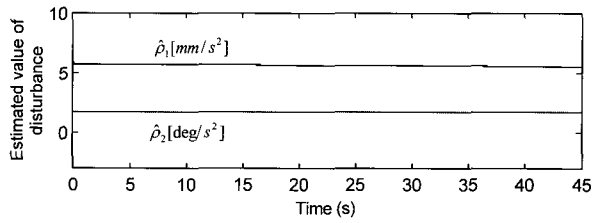

Fig. 23. Estimated values of disturbances $\hat{\rho}_1$[mm/s^2] and $\hat{\rho}_2$ [deg/s^2].

than during tracking on the straight line because the sliding mode is more effective on the arc line than on the straight line.

Fig. 17 shows the angular velocities of two wheels of the WMR. It shows that the vibration of angular velocities is larger for tracking an arc line than for

tracking a straight line. So Fig. 18 shows that the vibration of welding speed is larger for tracking the arc line than for tracking the straight line. The linear velocity of welding point in Fig. 18 is $v_w = v_r \pm 0.6mm/s$. In the practice of welding field, the error of welding velocity around $1.2mm/s$ is acceptable.

Fig. 19 shows that the value of sliding surface vector **s** converges to the average value of zero very fast during the welding process. The vector **s** have some stranger pulses at the position where the reference welding line is changed from straight line to curve or vice versa but it converges very rapidly to an average value of zero.

Figs. 20 and 21 show that the simulation and experimental results of control vector **u** are bounded and their average value converges to zero.

Fig. 22 shows that the linear velocity of controllable torch is zero and the length of torch slider is constant when error vector converges to zero. It means that the controllable torch acts as the fixed torch when error vector converges to zero.

Because the sliding surface vector has an average value of zero, by adaptation law in (25), the estimated values of disturbance converge to their constant value as shown in Fig. 23.

5. CONCLUSIONS

A nonlinear controller based on adaptive sliding-mode method which has a sliding surface vector including new boundizing function to enhance the tracking performances of the WMR has been introduced. The controller vector is robust and unsensitive in spite of uncertainties and external disturbances. To achieve the controller vector **u**, adaptation law vector and update law of the WMR are considered in view of a kinematic model and a dynamic model. The error configuration is defined and then sliding surface vector including new boundizing function is chosen. The error vector of system asymptotically converges to zero as reasonable as desired. A simple way of measuring the errors is also proposed. The stability of the system is considered in the sense of Lyapunov method. The simulation and experimental results show that the proposed controller can be applicable and implemented in the practical field.

REFERENCES

[1] M. Y. Kim, K. W. Ko, H. S. Cho, and J. H. Kim, "Visual sensing and recognition of welding environment for intelligent shipyard welding robots," *Proc. of IEEE Intelligent Robots and Systems*, vol. 3, pp. 2159-2165, 2000.

[2] Y. B. Jeon, S. S. Park, and S. B. Kim, "Modeling and motion control of mobile robot for lattice type of welding," *KSME International Journal*, vol. 16, No. 1, pp. 83-93, 2002.

[3] B. O. Kam, Y. B. Jeon, and S. B. Kim, "Motion control of two-wheeled welding mobile robot with seam tracking sensor," *Proc. of IEEE Industrial Electronics*, vol. 2, pp. 851-856, 2001.

[4] T. L. Chung, H. T. Bui, T. T. Nguyen, and S. B. Kim, "Sliding mode control of two-wheeled welding mobile robot for tracking smooth curved welding path," *KSME International Journal*, vol. 18, no. 7, pp. 1094-1106, 2004.

[5] J. M. Yang and J. H. Kim, "Sliding mode control for trajectory tracking of nonholonomic wheeled mobile robots," *IEEE Trans. on Robotics and Automation*, vol. 15, no. 3, pp. 578-587, 1999.

[6] T. H. Bui, T. L. Chung, T. T. Nguyen, and S. B. Kim, "A simple nonlinear control of a two-wheeled welding mobile robot," *International Journal of Control, Automation, and System*, vol. 1, no. 1, pp. 35-42, 2003.

[7] D. K. Chwa, J. H. Seo, P. J. Kim, and J. Y. Choi, "Sliding mode tracking control of nonholonomic wheeled mobile robots," *Proc. of the American Control Conference*, pp. 3991-3996, 2002.

[8] X. Yun and Y. Yamamoto, "Internal dynamics of a wheeled mobile robot," *Proc. of IEEE Intelligent Robots and Systems*, pp. 1288-1294, 1993.

[9] T. Fukao, H. Nakagawa, and N. Adachi, "Adaptive tracking control of a nonholonomic mobile robot," *IEEE Trans. on Robotics and Automation*, vol. 16, no. 5, pp. 609-615, 2000.

[10] T. C. Lee, C. H. Lee, and C. C. Teng, "Adaptive tracking control of nonholonomic mobile robot by computed torque", *Proc. of IEEE Decision and Control*, pp. 1254-1259, 1999.

[11] Y. Kanayama, Y. Kimura, F. Miyazaki, and T. Noguchi, "A stable tracking control method for a nonholonomic mobile robot," *Proc. of IEEE Intelligent Robots and Systems Workshop*, Japan, Vol. 3, pp. 1236-1241, 1991.

[12] J. J. E. Slotine and W. Li, *Applied Nonlinear Control*, Prentice-Hall International, Inc., pp. 122-125, 1991.

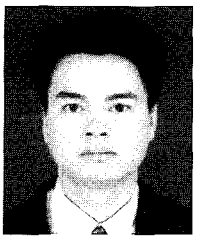

Ngo Manh Dung was born in Vietnam on January 27, 1974. He received the B.S. degree in the Faculty of Electrical and Electronics Engineering, Hochiminh City University of Technology, Vietnam in 1997. He received the M.S. and Ph.D. degrees in the Dept. of Mechanical Engineering, Pukyong National University, Busan, Korea in 2004 and 2007. He is a Lecturer of the Faculty of Electrical and Electronics Engineering, Hochiminh City University of Technology, Vietnam. His fields of interests are nonlinear control, power electronic and welding automation process.

Vo Hoang Duy was born in Vietnam on March 1, 1975. He received the B.S. and M.S. degrees in the Faculty of Electrical and Electronics Engineering, Hochiminh City University of Technology, Vietnam in 1997 and 2003. He is currently a Ph.D. student in the Dept. of Mechanical Engineering, Pukyong National University, Busan, Korea. His fields of interests are nonlinear control, mobile robot control and quadruped robot.

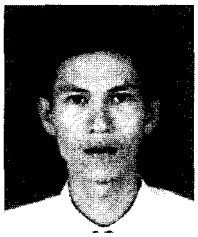

Nguyen Thanh Phuong was born in Vietnam on April 4, 1974. He received the B.S. and M.S. degrees in the Faculty of Electrical and Electronics Engineering, Hochiminh City University of Technology, Vietnam in 1998 and 2003. He is currently a Ph.D. student in the Dept. of Mechanical Engineering, Pukyong National University, Busan, Korea. His fields of interests are nonlinear control, mobile robot control and biped robot.

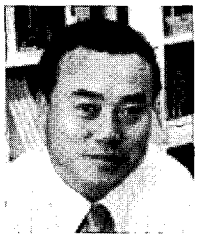

Sang Bong Kim was born in Korea on August 6, 1955. He received the B.S. and M.S. degrees from National Fisheries University of Busan, Korea, in 1978 and 1980. He received the Ph.D. degree in Tokyo Institute of Technology, Japan in 1988. After then, he is a Professor of Dept. of Mechanical Engineering, Pukyong National University, Busan, Korea. His research has been on robust control, biomechanical control, mobile robot control, biped robot and quadruped robot.

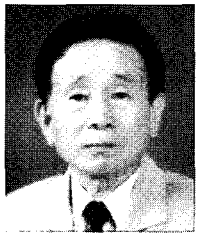

Myung Suck Oh was born in Korea on November 7, 1942. He received the M.S. and Ph.D. degrees from National Fisheries University of Busan, Korea in 1983 and 1994. He is a Professor of the Dept. of Mechanical Engineering, Pukyong National University, Busan, Korea. His research has been on Welding Engineering and Acoustic Emission.